

# essHi-C: Essential component analysis of Hi-C matrices

Stefano Franzini<sup>1</sup>, Marco Di Stefano<sup>2</sup>, and Cristian Micheletti<sup>1,\*</sup>

<sup>1</sup>SISSA, International School for Advanced Studies, Trieste, I-34136, Italy.

<sup>2</sup>CNAG-CRG, Centre Nacional d'Anàlisi Genòmica - Centre de Regulació Genòmica, Barcelona, 08028, Spain.

\*michelet@sisa.it

## Abstract

**Motivation:** Hi-C matrices are cornerstones for qualitative and quantitative studies of genome folding, from its territorial organization to compartments and topological domains. The high dynamic range of genomic distances probed in Hi-C assays reflects in an inherent stochastic background of the interactions matrices, which inevitably convolve the features of interest with largely aspecific ones.

**Results:** Here we introduce a discuss essHi-C, a method to isolate the specific, or essential component of Hi-C matrices from the aspecific portion of the spectrum that is compatible with random matrices. Systematic comparisons show that essHi-C improves the clarity of the interaction patterns, enhances the robustness against sequencing depth, allows the unsupervised clustering of experiments in different cell lines and recovers the cell-cycle phasing of single-cells based on Hi-C data. Thus, essHi-C provides means for isolating significant biological and physical features from Hi-C matrices.

## Introduction

Much of our current understanding of the structural-functional interplay in the genome owes to the advancements fostered by chromosome conformation capture-based methods (3C [1]), which are now numerous [2, 3]. For instance, Hi-C experiments demonstrated that inter-chromosome interactions are suppressed compared to intra-chromosome ones, thus giving quantitative support to the earlier notion of chromosome territories [4]. Inspection of the interaction matrices, and their dominant eigenvector [5], revealed the existence of two main chromatin compartments. Analysis of the interaction patterns showed the presence of self-interacting domains termed topologically associating domains (TADs) [6, 7, 8], which may form complex nested structures [9].

The increasing Hi-C resolution has made it possible to compare interaction patterns of different samples. The long term goal of such comparative studies is establishing which aspects of genome organisation are varied across different stages of cell development [10] and cell fate [11, 12, 13, 14], are affected by differences in gene transcription [15, 16, 17], or are mis-regulated in disease-related phenotypic alterations [18] and cancer [19].

Owing to the importance of comparative analysis, it is increasingly crucial to cross-validate data gathered with different protocols, resolution, and sequencing depth [20, 21, 22, 23, 24], thus identifying the common and statistically-significant features [25] in Hi-C matrices.

These observations pose, in turn, the more fundamental question of whether it is at all feasible to identify *a priori* the robust, significant features of a given Hi-C matrix without the necessity to resort to other terms of comparisons, which might contain biases or even not be available at all. An *a priori* knowledge of the significant features of a Hi-C matrix would also enhance the capability of detecting meaningful differences and similarities with other Hi-C matrices.

In this study, we show that spectral analysis methods, which rely on the information content of eigenvectors and eigenvalues, are ideally suited to this endeavour. However, with only a few exceptions, spectral methods have so far focussed on the first one or two eigenvectors of Hi-C matrices, which are informative for the chromatin compartmentalisation.

Here, we introduce *essHi-C* (after ‘essential Hi-C’) to extend these considerations to the full spectrum of Hi-C matrices, which we regularise for genomic distance. We show that most of the spectrum is compatible with that of random matrices, and thus represents an aspecific component shared across chromosomes from different samples. Interestingly, by discounting this aspecific part of the spectrum, and retaining only what we term the essential component, we enhance the definition of chromosomes’ architectural features and provide a significant advantage to readily pick up similarities of replicates and dissimilarity across different cell lines. Accordingly, heterogeneous sets of Hi-C matrices can be reliably grouped per cell lines using unsupervised clustering, which can even pick up the elusive interaction signatures of distinct experimental protocols. Finally, we show that essential matrices are stable against variations of the sequencing depth and the amount of input material of Hi-C. We found that *essHi-C* is predictive of the features discernible in Hi-C matrices with deeper sequencing and is informative for the genome architecture in extremely low-input Hi-C datasets, like the ones from single-cell Hi-C experiments.

## Methods

**Dataset.** Our dataset consist of intra-chromosome Hi-C matrices from 79 experiments of 9 human cell lines, including five with normal karyotype (GM12878, IMR90, NHEK, HMEC, hESC) and four with cancerous karyotypes (T47D, K562, KBM7, SKBR3) (see Supplementary Table 1). The *sra-toolkit* (<http://ncbi.github.io/sra-tools/>) (v2.9.6) was used to fetch the Hi-C datasets from the public sequence read archive (SRA) (Supplementary Table 1) and convert them to FASTQ format after validation. The TADbit pipeline [26] (<https://github.com/3DGenomes/tadbit>) was used to (i) check the quality of the FASTQ files; (ii) map the paired-end reads to the *H. sapiens* reference genome (release GRCh38/hg38) using GEM [27] accounting for restriction enzyme cut-sites; (iii) remove non-informative reads using the default TADbit filtering options; (iv) merge datasets within each experiment when appropriate; (v) normalise each experiment using the OneD method [28] at 100 kbp (kilo-basepairs) resolution.

**Observed over expected normalisation.** The obtained intra-chromosomal Hi-C matrices were subject to the so-called observed over expected (OoE) normalisation [5] to discount the overall dependence of matrix entries,  $A_{ij}$ , on the corresponding genomic distance,  $s = |i - j|$ . Starting from a OneD-normalised matrix,  $A$ , the average interactions at any genomic distance  $s$  was computed,  $I(s)$ . Each entry of the normalised matrix,  $B$ , is then defined as  $B_{ij} = \frac{A_{ij}}{I(s=|i-j|)}$ . Except when otherwise stated all Hi-C matrices considered in their full form are intended to be OoE-normalised.

**Random matrix ensemble.** As a null model for the OoE Hi-C matrices we considered the so-called Gaussian orthogonal ensemble, whose elements are symmetric matrices with entries drawn from a unitary Gaussian distribution, hence with zero mean and unit variance. On average, the salient spectral properties of the elements of this ensemble are as follows [29, 30]. The set of orthonormal eigenvectors sample uniformly the surface of a unit  $(N - 1)$ -sphere, where  $N$  is the linear size of the matrices. The generic component,  $x$ , of any eigenvector follows the same Gaussian distribution with zero mean and variance equal to  $1/N$ ,

$$p(x) = \sqrt{\frac{N}{2\pi}} e^{-\frac{Nx^2}{2}}. \quad (1)$$

The distribution of the eigenvalues,  $\lambda$ ’s, is governed by the Wigner’s semicircular law:

$$p(\lambda) = \frac{1}{2\pi\Lambda^2} \sqrt{4\Lambda^2 - \lambda^2} \quad (2)$$

with the interval  $[-\Lambda, \Lambda]$  being the support of  $\lambda$ .

**Essential component of Hi-C matrices.** One of our main results is that OoE Hi-C matrices have a spectrum largely consistent with that of random matrices, except for

a limited set of eigenvectors with atypically large eigenvalues in modulus. Borrowing a terminology introduced in other contexts [31, 32], we refer to these eigenspaces as *essential* and we use their spectral summation to define the essential Hi-C matrix. Starting from an OoE-normalised matrix,  $A$ , the entries of its essential form are defined as

$$A_{ij}^{ess} = \sum_{n=1}^{n^*} \lambda_n a_n^{(i)} a_n^{(j)}, \quad (3)$$

where  $a_n^{(i)}$  is the  $i$ -th component of the  $n$ -th eigenvector of  $A$  and  $\lambda_n$  is the associated eigenvalue. The matrix  $(a_n^{(i)} a_n^{(j)})$  denotes the projector associated to the eigenvector  $a$  (see Fig. 1D for examples). Once weighed for the correspondent eigenvalue  $(\lambda_n a_n^{(i)} a_n^{(j)})$ , it can be interpreted as the eigenspace, that is the contribution of  $a$  to the Hi-C contact pattern. The eigenspaces are ranked for decreasing modulus of the eigenvalues so that the summation is restricted to the top  $n^*$  essential spaces. In principle,  $n^*$  could be assigned differently for each matrix. For simplicity we set  $n^* = 10$  for all the applications in this study, except for the case of sparse single-cell Hi-C matrices, as the results do not vary appreciably upon including additional spaces, see Supplementary Fig. S1.

**Measuring matrix similarity across replicates.** In our dataset, the most numerous (34) independent Hi-C experiments on the same cell line (replicates) pertains to GM12878 cells. The similarity of these *a priori* equivalent Hi-C measurements was assessed as follows. For each chromosome (including autosomes and X) 100 pairs of replicate Hi-C matrices were randomly picked. For any such pair,  $P$  and  $Q$ , we next obtained the sum and difference matrices,  $S = P + Q$  and  $D = P - Q$ . The similarity parameter  $\gamma$  was computed as

$$\gamma = \frac{\langle S \rangle}{2\sigma_D} \quad (4)$$

where the angular brackets denote the average over the all entries  $S_{ij}$  with  $i \geq j$  and  $\sigma_D$  is the root mean-square value of all entries  $D_{ij}$ , again with  $i \geq j$ . OoE-normalised Hi-C matrices with good (poor) similarity thus yield values of  $\gamma$  that are much larger (smaller) than 1.

**Measuring matrix robustness across different sequencing depths.** We considered the set of GM12878 matrices from the experiment HIC003 [5], which have the highest available sequencing depth (see Supplementary Table 1), and used them as gold standard for comparisons with matrices at much lower depths. The consistency of a generic matrix with the gold standard (same chromosome) was measured in terms of the Spearman correlation coefficient of corresponding entries.

**Metric distance of essential Hi-C matrices.** For clustering purposes, the squared distance of two full OoE-normalised matrices,  $A$  and  $B$ , was computed as the Euclidian distance of corresponding entries,

$$d^2(A, B) = \sum_{i,j}^I |A_{ij} - B_{ij}|^2, \quad (5)$$

where the prime denotes that the sum is taken over  $i \geq j$ . The squared distance of the matrices in the essential form is instead defined as:

$$d^2(A_{ess}, B_{ess}) = \sum_{n < n^*} (\bar{\lambda}_n^2 + \bar{\mu}_n^2) - 2 \sum_{n,m < n^*} \bar{\lambda}_n \bar{\mu}_m (\mathbf{a}_n \cdot \mathbf{b}_m)^2, \quad (6)$$

where  $\mathbf{a}$  and  $\mathbf{b}$  are the eigenvectors of  $A$  and  $B$ , respectively,  $\lambda$  and  $\mu$  are the associated eigenvalues, and  $n^*$  is the spectral cutoff of eq. 3 for the essential component. The scaling factors  $\bar{\lambda}$  and  $\bar{\mu}$  make the distance robust respect to  $n^*$ , see Supplementary Fig. S1, and are defined as

$$\bar{\lambda}_n = \frac{\lambda_n}{\sum_{n < n^*} |\lambda_n|}, \quad \bar{\mu}_n = \frac{\mu_n}{\sum_{n < n^*} |\mu_n|}. \quad (7)$$

**Genome-wide distance of Hi-C matrices.** The genome-wide distance of all chromosomal matrices of two Hi-C experiments,  $\alpha$  and  $\beta$ , is defined as:

$$d(\alpha, \beta) = \left[ \sum_k d^2(M_{\alpha k}, M_{\beta k}) \right]^{1/2}, \quad (8)$$

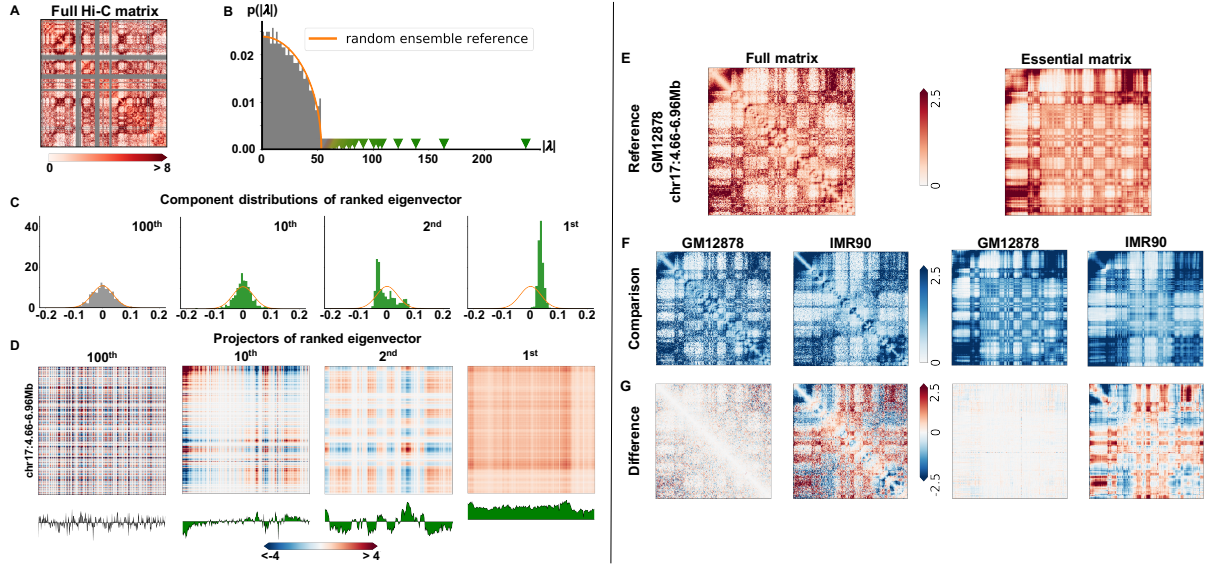


**Figure 1: Spectral properties of Hi-C vs random matrices and comparison of full and essential Hi-C matrices.** **A** Hi-C matrix of human chromosome 17 of cell line GM12878 (experiment HIC001) after OoE normalisation, see Methods. Grey bands correspond to the centromere and other regions removed by the TADbit filtering step (see Methods). Its eigenvalue distribution is shown in panel **B** along with the distribution for random unitary random matrices of same size (yellow). The outlier part of the Hi-C matrix spectrum,  $|\lambda| > 58.7$ , is highlighted in green. **C** Probability distributions for the components of Hi-C matrix eigenvectors of rank 1, 2, 10 and 100; analogous distribution for random matrix eigenvectors is shown in yellow. The spectral projectors of the Hi-C eigenvectors are shown in panel **D** for the region of chr17 between 4.66 and 9.69Mb. Below them the amplitude of the eigenvectors' components is shown. **E** Full Hi-C matrix of chromosome 17 from cell line GM12878 (experiment HIC001) and its essential version the genomic region chr17:4.66-6.96Mb is shown for clarity. **F** Other instances of full and essential matrices for the same genomic region for the same cell line (GM12878 from experiment HIC002) and a different ones (IMR90 from the experiment HIC050), see also Supplementary Table 1. The differences of these matrices with the reference ones of panel **E** are shown in panel **G**.

where index  $k$  runs over chromosomes, and  $M_{\alpha,k}$  is the Hi-C matrix of chromosome  $k$  from experiment  $\alpha$  and, depending on the context,  $d$  is either the plain Euclidian distance of eq. 5 or the essential one of eq. 6.

**Single cell Hi-C analysis.** The single-cell Hi-C (scHi-C) matrices in the haploid mouse embryonic stem cells (mESC) dataset of [33] was considered and analysed using the TADbit pipeline as for bulk Hi-C matrices with the exception of the OneD normalisation, which is not tailored for scHi-C matrices. After discarding assays with missing data for one or more chromosomes, our dataset consisted of 320 complete single cell assays covering three cellular stages labelled as G1, early-S, late-S/G2 in ref. [33], see Supplementary Table 2. Stages labelled as post-M and pre-M were not included because they contained zero and only one complete assay, respectively.

scHi-C matrices require suitable *ad hoc* extension of the essHi-C analysis used for standard (bulk) Hi-C matrices for their sparsity, which prevents taking meaningful OoE normalisations. For this preliminary application we identified the  $n^* = 50$  top ranking eigenspaces as the essential ones because they typically suffice to capture most of the trace of the non-normalised Hi-C matrices, see Supplementary Fig. S2. The same distance definition of eq. 6 was used for comparing essential scHi-C matrices and compute the ROC curves, where the G1, early-S, late-S/G2 labelling of [33] was used as gold standard.

The tripartite clustering of the essHiC dataset was computed from the Ward dendrogram.

## Results

### Spectral comparison of Hi-C and random matrices

Throughout the study we analysed Hi-C interaction matrices after the observed-over-expected (OoE) normalisation. As it is shown in the instance of Fig. 1A, the OoE normalisation, which discounts genomic-distance biases [5], puts on equal footing interactions at different sequence separations. The matrix in Fig. 1A pertains to chromosome 17 of cell line GM12878 and its spectral properties are illustrated in panels B-E. Specifically, panel B shows the probability distribution of the modulus of the eigenvalues,  $p(|\lambda|)$  while the probability distributions of the components of different ranking eigenvectors are shown in panel C. The same panels show, by contrast, the analogous quantities but computed for symmetric random matrices with the same linear size.

The two eigenvalues distributions are very closely matching throughout the range  $|\lambda| \leq 58.7$ , which covers 95% of the Hi-C spectrum. Within the  $|\lambda| \leq 58.7$  region, the well-matching spectral properties of Hi-C and random matrices also extends to eigenvectors. In fact, Their components are normally distributed, as for Gaussian random matrices, see panel C.

The outlying eigenvalues,  $|\lambda| > 58.7$ , are highlighted in green in panel B and accounts for only a small fraction of the Hi-C matrix spectrum. The components of the associated highest-ranking eigenvectors have a manifest non-Gaussian distribution. Thus, the top ranking eigenvalues and eigenvectors are the sole having markedly distincting properties from those found in random matrices. This fact holds in general, as it applies to different chromosomes and cell lines, see Supplementary Figs. S3 and S4, and thus establishes that the bulk of Hi-C matrix spectrum is largely compatible with that of random matrices, except for the small set of outlier eigenvalues and associated eigenvectors.

### Essential Hi-C matrices

Because the bulk of the spectrum of Hi-C matrices can be described by a statistical model informed solely by the linear size of the matrix, we discounted this aspecific component from the matrices so to isolate their *essential* component. The latter, that we term essential Hi-C matrix or *essHi-C* for brevity, is obtained from the spectral summation of the  $n^* = 10$  highest ranking projectors, see Methods and Fig. 1D.

A comparison of a full Hi-C matrix and its essential component is provided in Fig. 1E. The data are for the same entry of Fig. 1A, chromosome 17 and cell line GM12878, but are presented for a chromosome portion only to aid visualization. Remarkably, the essential matrix not only retains the distinctive contact patterns, but it presents them with greater clarity and contrast. The intra- and inter-domain contact patterns, as well as the domain boundaries, are more clearly defined too.

### Enhancement of specificity

The benefits of resorting to essential matrices, thus discounting the aspecific spectral component, further emerges from the comparative analysis of Fig. 1F, where the full and essential Hi-C matrices of panel A are compared with two other instances of chromosome 17, one from a biological replicate of the same GM12878 cell line, and one from the different IMR90 cell line.

The entry-by-entry subtraction of the matrices is presented in Fig. 1G and shows that contact pattern differences are sharper and more deeply marked for the essential matrices. Importantly, the difference matrix of GM12878 replicates presents as a uniform background while speckled patterns are clearly discernible for the full matrices of the different cell lines. The result holds generally and is not dependent on the considered cell types, see Supplementary Fig. S5.

### Robustness across replicates and varying sequencing depths

The enhancement of the contact pattern specificity is conveyed in Fig. 2A in terms of the similarity parameter  $\gamma$ . The latter quantifies how similar are corresponding entries in two

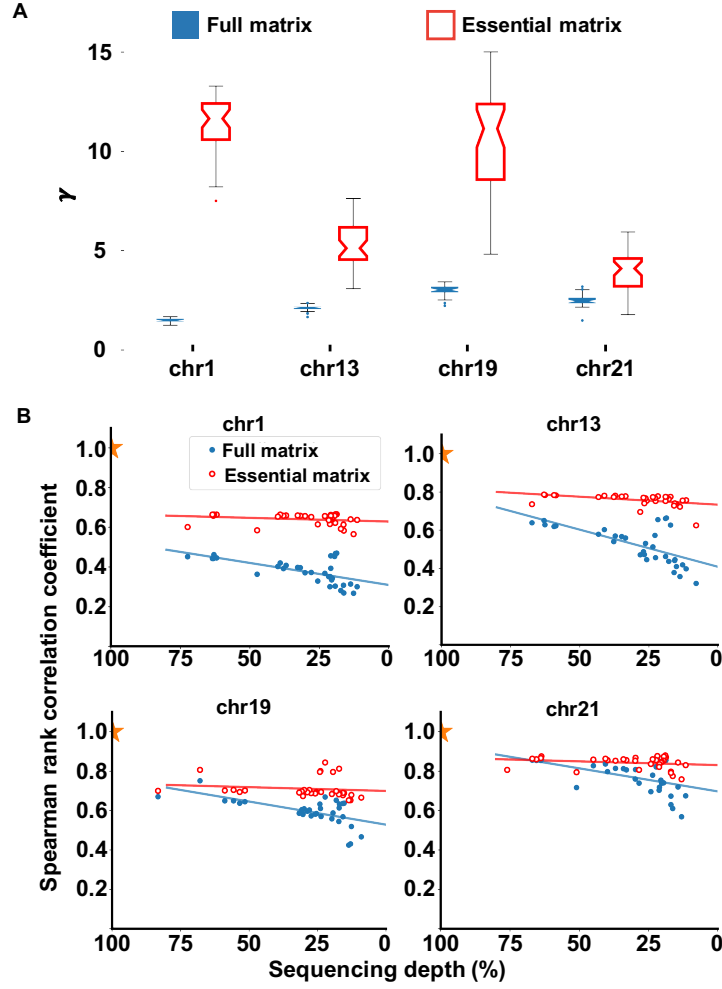


**Figure 2: Matrix robustness across replicates and sequencing depths.** **A** Box-whisker plots of the consistency parameter  $\gamma$ , see Methods, measured for distinct pairs of full and essential matrices for the GM12878 cell lines. Four chromosomes with large difference of length and gene density are considered. Boxplots show: central line, median; box limits, 75th and 25th percentiles; whiskers, 1.5 times the interquartile range; outliers beyond this range are shown as individual points. **B** Spearman rank correlation coefficient measured for corresponding entries of a high sequencing depth matrix (gold standard HIC003, 100% depth) and matrices at lower depths. Data are for the GM12878 and the same four chromosomes as in panel **A**.

matrices relative to their inherent statistical uncertainty, see Methods. Fig. 2A shows the distribution of  $\gamma$  computed for randomly picked pairs of GM12878 matrices for four chromosomes. These correspond to chromosomes 1, 13, 19 and 21, which were chosen for their diverse gene content and length.

The typical values of  $\gamma$  for full matrices are of the order unity and have a mild increasing dependence on chromosome length. Using, instead, the *essHi-C* version yields dramatic boost of the similarity parameter by about one order of magnitude, and with no particular bias or dependence on chromosome length (Fig. 2A).

We next examined the impact of the sequencing depth, taking as gold standard the full Hi-C matrices with the largest sequencing depth in the GM12878 dataset, see Supplementary Table 1. The Spearman’s rank correlation coefficient of corresponding entries of the gold standard and other matrices with lower depths are presented in Fig. 2B, again, for chromosomes 1, 13, 19 and 21.

Even though the gold standard is constituted by full Hi-C matrices the highest correlation across all four chromosomes and all lower depths is observed for the *essential* matrices, not the full ones. The result is general in that it holds for other chromosomes too, see Supplementary Fig. S6.

In addition, the correlation coefficient of the essential matrices has a visibly milder dependence on sequencing, the slope of the interpolating line being much smaller than the full case.

## Unsupervised clustering of different cell lines

As an application of the *essHi-C* analysis, we performed the unsupervised clustering of a heterogeneous dataset of 79 matrices, comprising (non-uniformly) 8 distinct cell lines and 3 different Hi-C techniques (Supplementary Table 1 and Methods).

The two clusterings obtained by using the full and essential matrices are shown as dendrograms in Fig. 3A,C. They present major and striking differences.

First, although the dendrograms are drawn using the same unit for the Ward score, the length of the branches for the essential matrices are more than twice longer (2.5 max Ward score) than the ones for full ones (1.0 max Ward score). This fact indicates that *essHi-C* matrices for more definite clusters compared to the full matrices.

The content of the clusters are also very different. In full matrices one can resolve the breast cancer (T47D) cell lines, whose chromosomal aberrations reflect in large-scale matrix changes [34]. However, other cell lines are poorly resolved, including the most numerous ones of GM12878 and IMR90, Fig. 3A.

The essential matrices return instead sharp subdivisions between different cell lines already from the early stages in the dendrogram hierarchy, see panel C. In addition, the associated pairwise distance matrix has a clear block structure, unlike the case of full matrices, see Fig. 3B,D.

The higher discriminatory power of *essHi-C* matrices is conveyed by the ROC curves shown in Fig. 3E. Full matrices yield an area-under-the-curve (AUC) parameter of 0.6, which only marginally improves with respect to the random reference ( $AUC = 0.5$ ). On the other hand essential matrices yield a nearly optimal performance, with  $AUC = 0.98$ .

As further terms of reference, Fig. 3E shows ROC curves obtained applying other methods to the full matrices. These include a Gaussian filter (convolution with unitary or single-bin variance), GenomeDISCO [25], and Hi-C Spector [35]. The Gaussian filter is often used as a means to curb noise in Hi-C matrices by averaging over neighbouring entries while the latter two methods are of interest here for they are based on the use of eigenspaces to compare Hi-C matrices. The AUC values for the Gaussian filter, Hi-C Spector and GenomeDisco are 0.90, 0.82 and 0.91, respectively, which are all significant. Some of these methods, including spectral ones, were purposely devised towards the comparative analysis of Hi-C matrices. The about optimal *essHi-C* performance is thus appealing as it is natively formulated as an enhancement method of individual matrices which can be adopted in comparative contexts too, as shown here.

By analyzing the quality of different numbers of groupings within the *essHiC* dendrogram, using the Dunn index, one discovers that the optimal number of clusters is 13, which is larger than the number of cell lines (9).

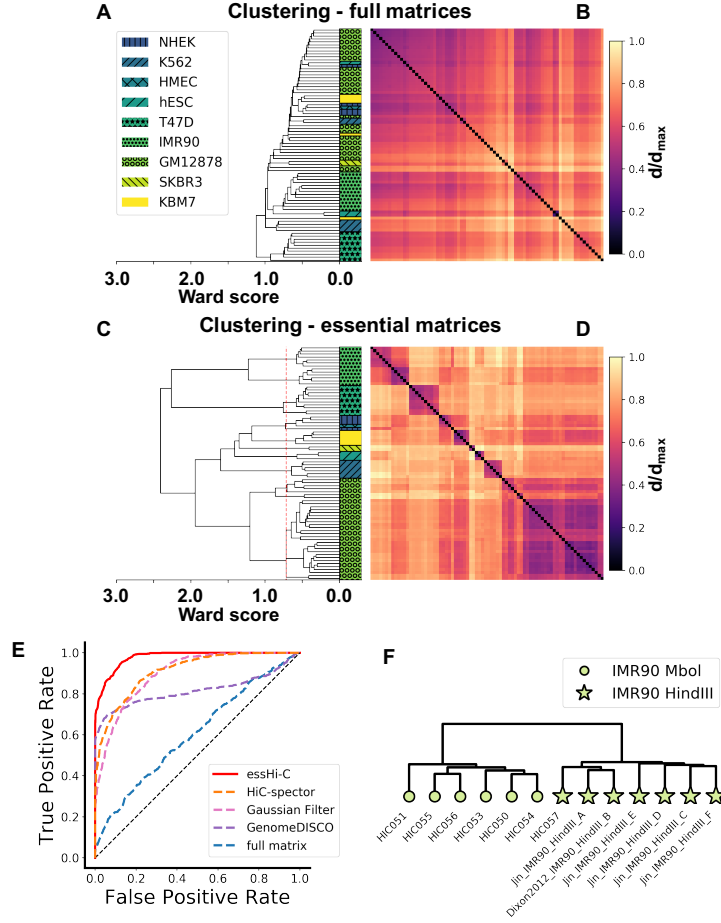


**Figure 3: Clustering of different cell lines** **A** Ward dendrogram of the dataset of 79 Hi-C experiments, covering different cell lines, based on the genome-wide distance of full Hi-C matrices. The pairwise distance matrix, with entries normalised to the maximum is shown in panel **B**. Analogous quantities, but computed for the corresponding essential Hi-C matrices are shown in panels **C** and **D**. The dashed line in the dendrogram of panel **C** marks the Ward score of the optimal (Dunn) subdivision in 13 clusters. The distances computed for the full and essential matrices, and other methods, were used to compute the ROC curves of panel **E**, where true positives correspond to instances of the same cell lines. **F** Section of the dendrogram in **D** regarding the IMR90 cell line, which shows the correlation with the used restriction enzymes.



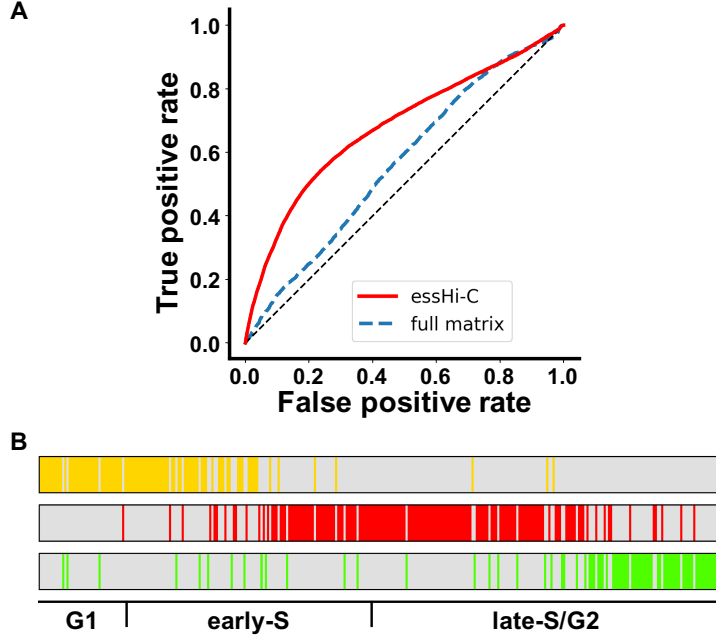


**Figure 4: Cell-phasing of single-cell Hi-C matrices.** **A** The distances of single-cell matrices from [33] in their full and essential forms were used to compute the ROC curves, where true positives correspond to instances with the same G1, early-S, late-S/G2 labelling of [33]. **B** The bands correspond to the tripartite clustering assignment of the essHi-C matrices. The entries follow the time ordering of [33].

All clusters except one contain one cell-type only, however, while all experiments of cell-types K562, hESC, SKBR3, and KBM7 are contained within a single cluster, other cell-types ensembles display a richer internal structure: this is apparent especially for IMR90 experiments, which are sharply divided into two clusters (Fig. 3F). Upon closer inspection one finds that this division is not an arbitrary one, but corresponds to different restriction enzymes and experimental techniques: one cluster contains *In-situ* experiments using Mbol, while the other are *dilution* Hi-C experiments using HindIII.

Other subdivisions within cell-lines are not as clear-cut and cannot be explained only in terms of different experimental methodologies. However one interesting case is given by the only mixed cluster, containing NHEK and HMEC experiments: both cell lines are epithelial samples, which may explain their similarity, moreover all experiments within the cluster share the same methodology (*In-situ*, Mbol). On the other hand the single isolated NHEK experiment is a *dilution* Hi-C, and uses the HindIII reduction enzyme.

### Single-cell Hi-C matrices

Lastly, we applied the essHi-C analysis to an entirely distinct Hi-C context, namely single-cell Hi-C (scHi-C). We considered the scHi-C set of ref. [33], which covers different cell-cycle stages of the mESC mouse embryonic cell line. In ref. [33] this data set time-ordered *a posteriori* with an elegant dimensional reduction procedure, which was instrumental to enhance the features of the inherently sparse matrices. To account for the sparsity of scHi-C matrices we performed the essential analysis using  $n^* = 50$  eigenspaces, see Methods and Supplementary Fig. S2.

The set of scHi-C matrices, in their plain form, cannot be clustered in a meaningful time-ordered way, as shown by the near-diagonal trend (blue line) in the ROC plot of Fig. 4 (AUC=0.55). The essHi-C matrices, instead, show a noticeable and significant correlation, AUC=0.68. Indeed, the same metrics and clustering procedure adopted for the ensemble Hi-C dataset of Fig. 3 returns primary partitions that are in very good accord with the time-ordered cellular stages proposed by [33], see Fig. 4B.

## Discussion

We presented a systematic spectral analysis of Hi-C matrices and established a general strategy to isolate their essential component from the largely-aspecific complementary one.

The starting point of the analysis was the comparison of the spectral properties of OoE-normalised Hi-C matrices with those of random matrices. For the latter we considered the Gaussian orthogonal ensemble, which is commonly taken as reference for the statistical spectral properties of systems with many degrees of freedom with complex interactions.

The comparison presented in Fig. 1 demonstrated that random matrices are viable terms of references for Hi-C matrices. In fact, the distributions of their eigenvalues and eigenvectors components are largely superposable, except for a small subset of outlier eigenspaces. It is this part of the spectrum, which stands out from the statistically-dominated background, that subsumes the specific features of the Hi-C data. We used to define the essential Hi-C matrix via the spectral summation that is algorithmically implemented in the `essHi-C` package.

The gist of the `essHi-C` analysis is different from approaches addressing data noise in Hi-C matrices at the local or bin-wise level. The latter, in fact, are designed to remove biological biases [36, 28] or numerical imbalance [37, 38] from Hi-C matrices, while `essHi-C` discounts the aspecific component by isolating the spectral, hence generally non-local properties that differ from random matrices.

The resulting enhanced specific content of the essential matrices is illustrated by the clearer and sharper features of essential matrices (Fig. 1 and, especially, by the comparison of different instances of Hi-C matrices from the same or different cell lines (Fig. 1G). The subtraction of matrices of the same cell lines is noticeably more uniform and less noisy for the essential matrices compared to the full ones. In addition, the subtraction of the `essHi-C` matrices of different cell lines provides a neater highlighting of the different features, which are instead convolved with noise in full matrices.

We focussed on two applications of the `essHi-C` analysis, chosen for their relevance and challenging nature. Firstly, we compared full Hi-C matrices obtained at high sequencing depth, with matrices at lower depth, both in the full and essential forms, see Fig. 2. The comparison demonstrated that essential matrices have a significant boost of correlation with the highest depth reference matrices. In fact, the correlation of the essential matrices is only modestly impacted by the decrease of the sequencing depth. These results provide a striking illustration of the significant potential that the `essHi-C` analysis for isolating specific interaction features that would require major increase of sequencing depth to be discerned in plain matrices.

Secondly, we carried out the unsupervised clustering of a heterogenous ensemble of Hi-C matrices covering several cell lines, see Fig. 3. Good correspondence of cell lines and the unsupervised hierarchical subdivisions are observed only for the `essHi-C` matrices, not the full ones. Furthermore, `essHi-C` based subdivisions of the IMR90 cell lines correlate with the different restriction enzymes used in the Hi-C assays for the two subsets. This unexpected result shows that different experimental probes can reflect in sufficiently distinct contact propensities, and that these can be picked up using `essHi-C` analysis.

Overall, the results show that `essHi-C` matrices are better suited than full matrices to isolate significant contact patterns, which ought to be useful also in context where contact propensities are used for chromosome modelling both to generate mean-field genome structures [39, 40] or to highlight the cell-to-cell variability [41, 42].

Finally, to illustrate the perspective potential of `essHi-C` analysis we discussed a preliminary application to single cell matrices, focussing on the set of ref. [33]. The ROC curves in Fig. 4 show that the time ordering of Nagano *et al.* cannot be recovered from the full scHi-C matrices. This is consistent with the fact that a dimensional-reduction of scHi-C matrices was needed to obviate to the sparsity of the two-dimensional full matrices and establish their time-ordering. It is therefore significant and appealing that, once the matrices are casted in their essential form, a clear correlation with the time ordering of ref. [33] emerges, and the main cellular phases are recovered, see Fig. 4. This fact, suggests that `essHi-C` analysis might be profitably used in place of the dimensional reduction step for a more direct determination of time-ordering or other scHi-C applications.

More in general, our results further emphasizes the advantages offered by `essHi-C` analysis

across very different contexts.

## Conclusion

We presented a systematic spectral analysis of Hi-C matrices and established a general strategy to identifying and separating their essential component from the largely aspecific complementary one.

By analysing essential Hi-C matrices in different contexts, we established numerous advantages over the use of spectral-complete (full) ones: from improving the sharpness and clarity of the specific interaction to enhancing the robustness against sequencing depth, allowing the unsupervised clustering of different cell lines and the cell-phasing of single-cell assays.

The results open numerous perspectives for using essHi-C analysis to optimally isolate biologically- and physically-relevant information from Hi-C matrices. Beyond the applications considered here, we expect our tool to be useful in comparative contexts where variations of chromosome compartmentalization could be picked up with enhanced reliability and hence better related to epigenomics changes [43] or cell differentiation [11, 12, 13].

The essHi-C software package is made freely available for academic use and can be accessed at <https://github.com/stefanofranzini/essHIC>.

## Funding

This work has been supported by the Italian Ministry for University.

## References

- [1] J. Dekker. Capturing chromosome conformation. *Science*, 295(5558):1306–1311, feb 2002.
- [2] Stefan Grob and Giacomo Cavalli. Technical review: a hitchhiker’s guide to chromosome conformation capture. In *Plant Chromatin Dynamics*, pages 233–246. Springer, 2018.
- [3] Nadine Übelmesser and Argyris Papantonis. Technologies to study spatial genome organization: beyond 3c. *Briefings in Functional Genomics*, 18(6):395–401, 2019.
- [4] T. Cremer and C. Cremer. Chromosome territories, nuclear architecture and gene regulation in mammalian cells. *Nature Reviews Genetics*, 2:292, 2001.
- [5] E. Lieberman-Aiden, N. L. van Berkum, L. Williams, M. Imakaev, T. Ragooczy, A. Telling, I. Amit, B. R. Lajoie, P. J. Sabo, M. O. Dorschner, R. Sandstrom, B. Bernstein, M. A. Bender, M. Groudine, A. Gnirke, J. Stamatoyannopoulos, L. A. Mirny, E. S. Lander, and J. Dekker. Comprehensive mapping of long-range interactions reveals folding principles of the human genome. *Science*, 326(5950):289–293, oct 2009.
- [6] T. Sexton, E. Yaffe, E. Kenigsberg, F. Bantignies, B. Leblanc, M. Hoichman, H. Parinello, A. Tanay, and G. Cavalli. Three-dimensional folding and functional organization principles of the drosophila genome. *Cell*, 148:458, 2012.
- [7] Jesse R. Dixon, Siddarth Selvaraj, Feng Yue, Audrey Kim, Yan Li, Yin Shen, Ming Hu, Jun S. Liu, and Bing Ren. Topological domains in mammalian genomes identified by analysis of chromatin interactions. *Nature*, 485(7398):376–380, apr 2012.
- [8] Elphège P. Nora, Bryan R. Lajoie, Edda G. Schulz, Luca Giorgetti, Ikuhiro Okamoto, Nicolas Servant, Tristan Piolot, Nynke L. van Berkum, Johannes Meisig, John Sedat, Joost Gribnau, Emmanuel Barillot, Nils Blüthgen, Job Dekker, and Edith Heard. Spatial partitioning of the regulatory landscape of the x-inactivation centre. *Nature*, 485(7398):381–385, apr 2012.
- [9] James Fraser, Carmelo Ferrai, Andrea M Chiariello, Markus Schueler, Tiago Rito, Giovanni Laudanno, Mariano Barbieri, Benjamin L Moore, Dorothee CA Kraemer, Stuart Aitken, Sheila Q Xie, Kelly J Morris, Masayoshi Itoh, Hideya Kawaji, Ines Jaeger, Yoshihide Hayashizaki, Piero Carninci, Alistair RR Forrest, Colin A Semple, Josée Dostie, Ana Pombo, and Mario Nicodemi. Hierarchical folding and reorganization of chromosomes are linked to transcriptional changes in cellular differentiation. *Molecular Systems Biology*, 11(12):852, dec 2015.
- [10] Hui Zheng and Wei Xie. The role of 3d genome organization in development and cell differentiation. *Nature Reviews Molecular Cell Biology*, page 1, 2019.
- [11] Boyan Bonev, Netta Mendelson Cohen, Quentin Szabo, Lauriane Fritsch, Giorgio L Papadopoulos, Yaniv Lubling, Xiaole Xu, Xiaodan Lv, Jean-Philippe Hugnot, Amos Tanay, et al. Multiscale 3d genome rewiring during mouse neural development. *Cell*, 171(3):557–572, 2017.
- [12] Ralph Stadhouders, Enrique Vidal, François Serra, Bruno Di Stefano, François Le Dily, Javier Quilez, Antonio Gomez, Samuel Collombet, Clara Berenguer, Yasmina Cuartero, et al. Transcription factors orchestrate dynamic interplay between genome topology and gene regulation during cell reprogramming. *Nature Genetics*, 50(2):238–249, 2018.
- [13] Jonas Paulsen, Tharvesh M Liyakat Ali, Maxim Nekrasov, Erwan Delbarre, Marie-Odile Baudement, Sebastian Kurscheid, David Tremethick, and Philippe Collas. Long-range interactions between topologically associating domains shape the four-dimensional genome during differentiation. *Nature Genetics*, 51(5):835–843, 2019.
- [14] Satish Sati, Boyan Bonev, Quentin Szabo, Daniel Jost, Paul Bensadoun, Francois Serra, Vincent Loubiere, Giorgio Lucio Papadopoulos, Juan-Carlos Rivera-Mulia, Lauriane Fritsch, et al. 4d genome rewiring during oncogene-induced and replicative senescence. *Molecular Cell*, 78(3):522 – 538.e9, 2020.
- [15] Job Dekker, Marc A. Marti-Renom, and Leonid A. Mirny. Exploring the three-dimensional organization of genomes: interpreting chromatin interaction data. *Nature Reviews Genetics*, 14(6):390–403, may 2013.

- [16] Tom Sexton and Giacomo Cavalli. The role of chromosome domains in shaping the functional genome. *Cell*, 160(6):1049–1059, mar 2015.
- [17] Anthony D. Schmitt, Ming Hu, Inkyung Jung, Zheng Xu, Yunjiang Qiu, Catherine L. Tan, Yun Li, Shin Lin, Yiing Lin, Cathy L. Barr, and Bing Ren. A compendium of chromatin contact maps reveals spatially active regions in the human genome. *Cell Reports*, 17(8):2042–2059, nov 2016.
- [18] Darío G. Lupiáñez, Katerina Kraft, Verena Heinrich, Peter Krawitz, Francesco Brancati, Eva Klopocki, Denise Horn, Hülya Kayserili, John M. Opitz, Renata Laxova, Fernando Santos-Simarro, Brigitte Gilbert-Dussardier, Lars Wittler, Marina Borschirwer, Stefan A. Haas, Marco Osterwalder, Martin Franke, Bernd Timmermann, Jochen Hecht, Malte Spielmann, Axel Visel, and Stefan Mundlos. Disruptions of topological chromatin domains cause pathogenic rewiring of gene-enhancer interactions. *Cell*, 161(5):1012–1025, may 2015.
- [19] Peter Hugo Lodewijk Krijger and Wouter De Laat. Regulation of disease-associated gene expression in the 3d genome. *Nature Reviews Molecular Cell Biology*, 17(12):771, 2016.
- [20] Jean-Philippe Fortin and Kasper D. Hansen. Reconstructing A/B compartments as revealed by Hi-C using long-range correlations in epigenetic data. *Genome Biology*, 16(1), aug 2015.
- [21] Tao Yang, Feipeng Zhang, Galip Gürkan Yardımcı, Fan Song, Ross C. Hardison, William Stafford Noble, Feng Yue, and Qunhua Li. HiCRep: assessing the reproducibility of hi-c data using a stratum-adjusted correlation coefficient. *Genome Research*, 27(11):1939–1949, aug 2017.
- [22] John C. Stansfield, Kellen G. Cresswell, Vladimir I. Vladimirov, and Mikhail G. Dozmorov. HiCcompare: an r-package for joint normalization and comparison of HI-c datasets. *BMC Bioinformatics*, 19(1), jul 2018.
- [23] Galip Gürkan Yardımcı, Hakan Ozadam, Michael EG Sauria, Oana Ursu, Koon-Kiu Yan, Tao Yang, Abhijit Chakraborty, Arya Kaul, Bryan R Lajoie, Fan Song, et al. Measuring the reproducibility and quality of hi-c data. *Genome Biology*, 20(1):57, 2019.
- [24] Jingtian Zhou, Jianzhu Ma, Yusi Chen, Chuankai Cheng, Bokan Bao, Jian Peng, Terrence J. Sejnowski, Jesse R. Dixon, and Joseph R. Ecker. Robust single-cell hi-c clustering by convolution- and random-walk-based imputation. *Proceedings of the National Academy of Sciences*, 116(28):14011–14018, jun 2019.
- [25] Oana Ursu, Nathan Boley, Maryna Taranova, Y X Rachel Wang, Galip Gurkan Yardımcı, William Stafford Noble, and Anshul Kundaje. GenomeDISCO: a concordance score for chromosome conformation capture experiments using random walks on contact map graphs. *Bioinformatics*, 34(16):2701–2707, mar 2018.
- [26] François Serra, Davide Baù, Mike Goodstadt, David Castillo, Guillaume J. Filion, and Marc A. Marti-Renom. Automatic analysis and 3d-modelling of hi-c data using TADbit reveals structural features of the fly chromatin colors. *PLOS Computational Biology*, 13(7):e1005665, jul 2017.
- [27] Santiago Marco-Sola and Paolo Ribeca. Efficient Alignment of Illumina-Like High-Throughput Sequencing Reads with the GENomic Multi-tool (GEM) Mapper. *Current Protocols in Bioinformatics*, 50(1):11–13, 2015.
- [28] Enrique Vidal, François le Dily, Javier Quilez, Ralph Stadhouders, Yasmina Cuartero, Thomas Graf, Marc A Marti-Renom, Miguel Beato, and Guillaume J Filion. Oned: increasing reproducibility of hi-c samples with abnormal karyotypes. *Nucleic Acids Research*, 46(8):e49–e49, 2018.
- [29] Sean O'Rourke, Van Vu, and Ke Wang. Eigenvectors of random matrices: A survey. *Journal of Combinatorial Theory, Series A*, 144:361–442, nov 2016.
- [30] Giacomo Livan, Marcel Novaes, and Pierpaolo Vivo. *Introduction to Random Matrices*. Springer International Publishing, 2018.

- [31] Andrea Amadei, Antonius BM Linssen, and Herman JC Berendsen. Essential dynamics of proteins. *Proteins: Structure, Function, and Bioinformatics*, 17(4):412–425, 1993.
- [32] Cristian Micheletti. Comparing proteins by their internal dynamics: Exploring structure–function relationships beyond static structural alignments. *Physics of life reviews*, 10(1):1–26, 2013.
- [33] Takashi Nagano, Yaniv Lubling, Csilla Várnai, Carmel Dudley, Wing Leung, Yael Baran, Netta Mendelson Cohen, Steven Wingett, Peter Fraser, and Amos Tanay. Cell-cycle dynamics of chromosomal organization at single-cell resolution. *Nature*, 547(7661):61–67, 2017.
- [34] Milena Rondón-Lagos, Ludovica Verdun Di Cantogno, Caterina Marchiò, Nelson Rangel, Cesar Payan-Gomez, Patrizia Gugliotta, Cristina Botta, Gianni Bussolati, Sandra R Ramírez-Clavijo, Barbara Pasini, et al. Differences and homologies of chromosomal alterations within and between breast cancer cell lines: a clustering analysis. *Molecular Cytogenetics*, 7(1):8, 2014.
- [35] Koon-Kiu Yan, Galip Gürkan Yardımcı, Chengfei Yan, William S Noble, and Mark Gerstein. HiC-spector: a matrix library for spectral and reproducibility analysis of hi-c contact maps. *Bioinformatics*, 33(14):2199–2201, 2017.
- [36] Eitan Yaffe and Amos Tanay. Probabilistic modeling of hi-c contact maps eliminates systematic biases to characterize global chromosomal architecture. *Nature Genetics*, 43(11):1059–1065, oct 2011.
- [37] Maxim Imakaev, Geoffrey Fudenberg, Rachel Patton McCord, Natalia Naumova, Anton Goloborodko, Bryan R Lajoie, Job Dekker, and Leonid A Mirny. Iterative correction of hi-c data reveals hallmarks of chromosome organization. *Nature Methods*, 9(10):999–1003, sep 2012.
- [38] P. A. Knight and D. Ruiz. A fast algorithm for matrix balancing. *IMA Journal of Numerical Analysis*, 33(3):1029–1047, oct 2012.
- [39] Marie Trussart, François Serra, Davide Baù, Ivan Junier, Luis Serrano, and Marc A Marti-Renom. Assessing the limits of restraint-based 3d modeling of genomes and genomic domains. *Nucleic Acids Research*, 43(7):3465–3477, 2015.
- [40] François Serra, Marco Di Stefano, Yannick G Spill, Yasmina Cuartero, Michael Goodstadt, Davide Baù, and Marc A Marti-Renom. Restraint-based three-dimensional modeling of genomes and genomic domains. *FEBS letters*, 589(20):2987–2995, 2015.
- [41] Luca Giorgetti, Rafael Galupa, Elphège P Nora, Tristan Piolot, France Lam, Job Dekker, Guido Tiana, and Edith Heard. Predictive polymer modeling reveals coupled fluctuations in chromosome conformation and transcription. *Cell*, 157(4):950–963, 2014.
- [42] Harianto Tjong, Wenyan Li, Reza Kalhor, Chao Dai, Shengli Hao, Ke Gong, Yonggang Zhou, Haochen Li, Xianghong Jasmine Zhou, Mark A Le Gros, et al. Population-based 3d genome structure analysis reveals driving forces in spatial genome organization. *Proceedings of the National Academy of Sciences*, 113(12):E1663–E1672, 2016.
- [43] R. Vilarrasa-Blasi, P. Soler-Vila, N. Verdaguer-Dot, N. Russinol, M. Di Stefano, V. Chapaprieta, G. Clot, I. Farabella, P. Cusco, X. Agirre, F. Prosper, R. Beekman, S. Bea, D. Colomer, I. Gut, H. Stunnenberg, E. Campo, M.A. Marti-Renom, and J.I. Martin-Subero. Dynamics of genome architecture and chromatin function during human b cell differentiation and neoplastic transformation. *Nature Communications*, in press, 2020.